Version of Record: https://www.sciencedirect.com/science/article/pii/S004565352201431X
Manuscript_f29789a6b42a0c34827f863059293f87

PFAS Concentrations in Soil Versus Soil Porewater: Mass Distributions and the Impact of Adsorption at Air-Water Interfaces

M.L. Brusseau[1,2,*] and B. Guo[2]

[1]Environmental Science Department

[2]Hydrology and Atmospheric Sciences Department

The University of Arizona

Tucson, AZ 85721

Submitted for Review in:

Chemosphere

February 2022

Revised April 28, 2022

[*]Corresponding author, Brusseau@arizona.edu

PFAS Concentrations in Soil Versus Soil Porewater: Mass Distributions and the Impact of Adsorption at Air-Water Interfaces

M.L. Brusseau[1,2,*] and B. Guo[2]

[1]Environmental Science Department

[2]Hydrology and Atmospheric Sciences Department

The University of Arizona

Tucson, AZ 85721

Submitted for Review in:

Chemosphere

February 2022

Revised April 28, 2022

[*]Corresponding author, Brusseau@arizona.edu

ABSTRACT

Determining the risk posed by PFAS leaching from soil to groundwater requires quantification of the magnitude and temporal/spatial variability of PFAS mass discharge from the vadose zone, which is governed in part by the concentrations of PFAS in soil porewater. Porewater concentrations are impacted and mediated by the properties of the PFAS and soil, multiple transport and fate processes, and site conditions. The objective of this research was to delineate the relationship between soil porewater concentrations and soil concentrations, based on a comprehensive model of PFAS mass distribution within a soil sample volume. Measured parameters representing solid-phase sorption and air-water interfacial adsorption are used to illustrate the impact of soil and PFAS properties on the distribution of representative PFAS between soil and soil porewater. Literature data reported for soil and soil porewater concentrations of several PFAS obtained from outdoor lysimeter experiments are used to test the distribution model. Soil-to-porewater concentration ratios predicted with the model compared very well to the measured concentration ratios. The nondimensional distribution coefficient that describes the distribution of PFAS mass amongst all domains within a soil sample was observed to be a function of PFAS molecular size. Numerical simulations conducted for a model fire-training source area were used to illustrate the ranges in magnitude of soil versus porewater concentrations for representative field conditions. The results of the measured and simulated data sets demonstrated the importance of air-water interfacial adsorption for the distribution of the longer-chain PFAS within soil samples. PFAS soil porewater concentrations are anticipated to range from ng/L to mg/L depending upon soil concentrations, which in turn depend upon the nature of the site.

Keywords: PFOS; PFOA; Perfluorinated; Sorption; Air-water Interfacial adsorption; Leaching

1. Introduction

Per and polyfluoroalkyl substances (PFAS) have been demonstrated to be widespread in soils across the globe (Brusseau et al., 2020). PFAS concentrations are often, but not always, observed to be highest near the surface and to diminish with depth. This is particularly the case for longer-chain PFAS. This distribution has been observed for different types of source sites, including sites impacted by fire-fighting foam applications (Filipovic et al., 2015; Baduel et al., 2017; Dauchy et al., 2019; Brusseau et al., 2020), manufacturing facilities (Davis et al. 2007), and land application of biosolids (Washington et al., 2010; Sepulvado et al. 2011; Pepper et al., 2021; Johnson, 2022). In addition, the concentrations of PFAS in soils are typically significantly higher than those in underlying groundwater, often by orders of magnitude (Anderson et al., 2019; Brusseau et al., 2020). These observations demonstrate that soils are a primary reservoir of PFAS at numerous sites. A critical concern for these sites is the potential for leaching of PFAS from soil, through the vadose zone, to groundwater, as illustrated by field-site investigations (Xiao et al., 2015; Baduel et al., 2017; Weber et al., 2017; Hoisaeter et al., 2019; Dauchy et al., 2019) and mathematical-modeling studies (Guo et al., 2020; Silva et al., 2020; Zeng et al., 2021).

The transport of PFAS in soils and the vadose zone is complex, as it is influenced by several potentially nonlinear, rate-limited interconnected processes. Transport experiments, mathematical-modeling studies, and field investigations have for example illustrated the impacts of solid-phase sorption, adsorption at air-water interfaces, and precursor transformation on PFAS migration (e,g., Gellrich et al., 2012; Vierke et al., 2014; Lyu et al., 2018; Brusseau et al., 2019a, 2019b; Hoisaeter et al., 2019; McLachlan et al., 2019; Guelfo et al., 2020; Guo et al., 2020; Silva et al., 2020; Brusseau et al., 2021; Nickerson et al., 2021). Determining the risk posed by PFAS leaching to groundwater requires quantification of the magnitude and temporal/spatial variability

of PFAS mass discharge from the vadose zone. This mass discharge is governed by fluid discharge and the concentrations of PFAS in soil porewater, the latter of which is mediated by operative retention and transformation processes.

PFAS soil porewater concentrations and associated mass discharge can be quantified through the application of mathematical models. Comprehensive models that incorporate mechanistic representations of all relevant processes are important for determining the impact and importance of the various processes influencing transport. However, their application requires significant information for parameter input, which is not always practical. An alternative is the use of screening-level models that have reduced input requirements. For example, a screening model employing analytical solutions for predicting long-term leaching of PFAS has been recently developed (Guo et al., 2022). While the level of input is reduced, there remains the need for characterization efforts to supply required parameters.

Direct measurement of PFAS concentrations in soil porewater is an alternative approach for characterizing mass discharge (Anderson et al., 2021; Quinnan et al., 2021). Porewater sampling can be used in lieu of, or preferably in conjunction with, mathematical modeling for site characterization. Effective use of porewater concentration data requires an understanding of the distribution of PFAS mass within a volume element of soil, and the relationship between soil and porewater concentrations. This relationship is more complex for PFAS compared to most other types of solutes due to the adsorption of PFAS at air-water interfaces, and the dependence of air-water interfacial area on water content and soil properties. This relationship between soil and soil porewater concentrations has not yet been investigated.

The objective of this research is to delineate the relationship between soil porewater concentrations and soil concentrations, based on a comprehensive model of PFAS mass

distribution within a soil sample volume. Measured parameters representing solid-phase sorption and air-water interfacial adsorption are used to illustrate the impact of soil and PFAS properties on the distribution of PFAS between soil and soil porewater. Literature data reported for soil and soil porewater concentrations of several PFAS obtained from outdoor lysimeter experiments are used to test the distribution model. Soil-to-porewater concentration ratios predicted with the model are compared to the measured concentration ratios. Numerical simulations conducted for a model fire-training source area are used to illustrate the magnitude of soil versus porewater concentrations for representative field conditions. The importance of air-water interfacial adsorption for mediating the distribution of PFAS within a soil sample is examined using the simulated and measured data sets.

2. Theory

We are interested in the distribution of PFAS among all possible domains within a volume sample of soil in the presence of a variety of phases including air (soil atmosphere), water (porewater), solids, nonaqueous-phase liquid (NAPL), and colloidal and other suspended and dissolved matter. This distribution is described and quantified using the comprehensive retention model of Brusseau (Brusseau, 2018; Brusseau et al., 2019a). The total mass of a select PFAS constituent in a volume of soil is given by:

$$M_t = C_p V_p + C_s M_s + C_a V_a + C_n V_n + C_{aw} A_{aw} + C_{nw} A_{nw} + C_{an} A_{an} + C_c M_c \quad [1]$$

where M_t is total mass in the volume of sample (M), C_p is the porewater concentration (M/L^3), C_s represents the mass of PFAS sorbed by the soil solids (soil-solids concentration, M/M), C_a is the concentration in the soil atmosphere (M/L^3), C_n is the concentration in NAPL present in the sample (M/L^3), C_{aw} represents the mass adsorbed at the air-water interface (air-water interfacial

concentration (M/L^2), C_{nw} represents the mass adsorbed at the NAPL-water interface (NAPL-water interfacial concentration (M/L^2), C_{an} represents the mass adsorbed at the air-NAPL interface (air-NAPL interfacial concentration (M/L^2), C_c represents the mass associated with colloidal and other suspended and dissolved matter in solution (M/M), A_{aw} is the total air-water interfacial area (L^2), A_{nw} is the total NAPL-water interfacial area (L^2), A_{an} is the total air-NAPL interfacial area (L^2), V_w is the volume of porewater (L^3), V_a is the volume of air (L^3), V_n is the volume of NAPL (L^3), M_s is the mass of soil solids (M), and M_c is the mass of colloidal material (M).

Normalizing the phase volumes, phase masses, and interfacial areas by the total sample volume, V_t, and introducing the equilibrium distribution coefficients results in transformation of equation 1 to:

$$M_t = C_p \theta_w V_t \left(1 + K_{d*}\frac{\rho_b}{\theta_w} + K_a\frac{\theta_a}{\theta_w} + K_n\frac{\theta_n}{\theta_w} + K_{aw*}\frac{a_{aw}}{\theta_w} + K_{nw*}\frac{a_{nw}}{\theta_w} + K_{an*}\frac{a_{an}}{\theta_w} + K_{c*}X_c\right) \quad [2]$$

where K_{d*} is the nonlinear solid-phase adsorption coefficient (cm^3/g), K_n is the NAPL-water partition coefficient (-), K_a is the air-water partition coefficient (Henry's coefficient, -), K_{aw*} is the nonlinear air-water interfacial adsorption coefficient (cm^3/cm^2), K_{nw*} is the nonlinear NAPL-water interfacial adsorption coefficient (cm^3/cm^2), K_{an*} is the nonlinear air-NAPL interfacial adsorption coefficient (cm^3/cm^2), K_{c*} is the nonlinear distribution coefficient for sorption by the colloids (cm^3/g), a_{aw} is the specific air-water interfacial area (cm^2/cm^3), a_{nw} is the specific NAPL-water interfacial area (cm^2/cm^3), a_{an} is the specific air-NAPL interfacial area (cm^2/cm^3), ρ_b is porous-medium bulk density (g/cm^3), θ_a is volumetric air content (cm^3/cm^3), θ_n is volumetric NAPL content (cm^3/cm^3), and θ_w is volumetric water content (cm^3/cm^3). By phase balance, $\theta_w + \theta_a + \theta_n = n$, where n is porosity. Note that X_c is the concentration of colloidal material in porewater (g/cm^3), defined as:

$$X_c = \frac{M_c}{\theta_w V_t} = \frac{M_c}{V_p} \quad [3]$$

Both solid-phase sorption and fluid-fluid interfacial adsorption of PFAS may be nonlinear under certain conditions. The nonlinearity of solid-phase sorption is often represented with the Freundlich isotherm. With this approach, the impact of nonlinearity on the magnitude of sorption can be represented by $K_{d*} = K_f C_{p0}^{(N-1)}$, where K_f and N are the Freundlich coefficients and C_{p0} is the aqueous concentration of interest. This approach may also be applied to sorption by colloidal matter. When sorption is linear, $K_{d*} = K_d$ and $K_{c*} = K_c$, where the coefficients without asterisks represent constants. A standard approach for representing nonlinear fluid-fluid interfacial adsorption is through use of the Szyszkowski-Langmuir equation, which leads to (using the air-water system as the example): $K_{aw*} = \Gamma_m/(C_p+a)$, where Γ_m is the maximum surface excess (=γ_0b/RT), R is the universal gas constant, T is temperature, γ_0 is the surface tension when C_p is zero, and a and b are constants from the Szyszkowski equation that describes surface tension as a function of aqueous concentration. This treatment can also be applied to represent nonlinear NAPL-water and air-NAPL interfacial adsorption processes. Fluid-fluid interfacial adsorption may be treated as linear at lower concentrations (e.g., Brusseau et al., 2021). Under these conditions, $K_{aw*} = K_{aw}$, $K_{nw*} = K_{nw}$, and $K_{an*} = K_{an}$, where the coefficients without asterisks represent constants. The specific concentrations at which fluid-fluid interfacial adsorption may be treated as linear depends upon the particular PFAS and properties of the porewater solution (Brusseau, 2019a). Partitioning between bulk water, NAPL, and air phases is commonly treated as linear.

The terms in parentheses in equation 2 can be defined as the nondimensional distribution coefficient, denoted as R_d:

$$R_d = \left(1 + K_{d*}\frac{\rho_b}{\theta_w} + K_a\frac{\theta_a}{\theta_w} + K_n\frac{\theta_n}{\theta_w} + K_{aw*}\frac{a_{aw}}{\theta_w} + K_{nw*}\frac{a_{nw}}{\theta_w} + K_{an*}\frac{a_{an}}{\theta_w} + K_{c*}X_c\right) \quad [4]$$

This term is very similar to the retardation factor developed for aqueous-phase transport of PFAS undergoing retention by all of the relevant processes (Brusseau et al., 2019a). The one difference is the treatment of PFAS mass associated with colloidal matter suspended or dissolved in porewater, which was incorporated into the mobile solution phase for development of the retardation factor for transport. With the introduction of R_d, equation 2 becomes:

$$M_t = C_p \theta_w V_t R_d \qquad [5]$$

The total concentration of the select PFAS, C_t (M/M), is defined as M_t/M_s. Substituting equation 5 gives:

$$C_t = \frac{C_p \theta_w R_d}{\rho_b} \qquad [6]$$

The ratio of total concentration to porewater concentration is therefore:

$$\frac{C_t}{C_p} = \frac{\theta_w}{\rho_b} R_d \qquad [7]$$

Inspection of equation 7 reveals that R_d represents the ratio of total mass present in the soil sample to the mass present as dissolved solute in porewater. The $\frac{\theta_w}{\rho_b}$ term represents the ratio of porewater volume to soil-solids mass and can be thought of as a unit conversion term. Note that the $\frac{C_t}{C_p}$ term has units of L^3/M. A dimensionless ratio can be developed by use of a volume-based total concentration, C_{tv} (M/L^3), defined as M_t/V_t. C_t and C_{tv} are related by the soil bulk density. C_t is the focus of the present study given that mass-based soil concentrations are the reporting standard.

Equations 2 and 4-7 represent all possible phases in which PFAS can potentially reside within a soil sample. However, several of the phases are unlikely to be relevant for many conditions. For example, many PFAS of concern have low vapor pressures and are thus not

161 measurably present in the vapor phase. In addition, many sites are unlikely to have NAPL
162 present in the vadose zone. Inspection of equation 2 shows that the impact of retention by
163 sorption to colloidal material in porewater will be relatively insignificant for moderate to low
164 concentrations of colloids and for smaller sorption coefficients. Under these preceding
165 conditions, R_d can be simplified to:

166 $$R_d = \left(1 + K_{d*}\frac{\rho_b}{\theta_w} + K_{aw*}\frac{a_{aw}}{\theta_w}\right) \qquad [8]$$

167 Examining this reduced form will be the focus of the present investigation.

168

169 **3. Methods**

170 This study comprises four components. For the first component, the ratio of total soil
171 concentration to soil porewater concentration as a function of water saturation will be
172 investigated for representative primary PFAS of concern. This will be accomplished by using
173 measured and estimated parameter values to calculate R_d values using equation 8, and then using
174 these values in equation 7. Three perfluorocarboxylic acids (PFCAs) of different chain length
175 will be used to examine chain-length effects. These three are perfluorobutanoic acid (PFBA),
176 perfluorooctanoic acid (PFOA), and perfluorotridecanoic acid (PFTDA). Perfluorooctane
177 sulfonic acid (PFOS) will also be included in the analysis. A natural sand will be used as the
178 porous medium for these calculations to focus on the impact of air-water interfacial adsorption.
179 Measured values for a_{aw} are available for this sand from our prior experiments (Brusseau and
180 Guo, 2021), as are K_d and K_{aw} values for the selected PFAS (Van Glubt et al., 2021). These
181 values are reported in Tables 1 and 2. The calculations are conducted employing constant K_{aw}
182 values, representing systems with PFAS concentrations in the µg/L range or lower.

183 The second component focuses on determining C_t/C_p ratios for PFOS as a function of
184 water saturation for three porous media for which PFOS has different magnitudes of solid-phase
185 sorption and that have different magnitudes of air-water interfacial area. Measured values for a_{aw}
186 are available for the three media from our prior experiments (Brusseau and Guo, 2021; El Ouni
187 et al., 2021), and are reported in Table 2. Measured K_d values for PFOS for the three media are
188 reported in Table 1. Freundlich N values reported for sorption of PFCAs by soils and sediments
189 are typically in the range of 0.7-1 (see recent compilation reported in Van Glubt et al., 2021),
190 thereby exhibiting relatively moderate nonlinearity. Hence, solid-phase sorption will be treated
191 as linear for the purposes of the first and second components. This treatment has minimal impact
192 on the results.
193 The third component of the study employs literature data reported for soil and soil
194 porewater concentrations of several PFAS obtained from outdoor lysimeter experiments
195 (Felizeter et al. 2021). These measured data are used to test the distribution model by comparing
196 soil-to-porewater concentration ratios predicted with the model to the measured concentration
197 ratios. Four edible crops (radish, lettuce, pea, and maize) were grown in outdoor lysimeters
198 packed with soil spiked with a mixture of 13 PFAS at 4 concentrations (nominal 0.1, 1, 5, and 10
199 mg/kg-dw for each PFAS). The PFAS mixture comprised 11 PFCAs, PFOS, and perfluorobutane
200 sulfonic acid (PFBS). The lysimeters were installed in the ground outside, and subject to natural
201 precipitation events as well as additional irrigation. PFAS concentrations were measured in soil,
202 soil porewater, and different plant tissues at harvest. Soil water contents were also reported.
203 Values for R_d defined in equation 8 were determined using measured and estimated
204 parameter values as follows. The soil employed has an organic-carbon content of 1%. Prior
205 research has indicated that soil organic carbon generally controls sorption of PFCAs and PFOS

206 for soils and sediments with organic-carbon contents in this range and higher (e.g., Higgins and
207 Luthy, 2006; Milinovic et al., 2015; Brusseau et al., 2019b). Therefore, K_d values were estimated
208 from the standard $K_d = K_{oc}\ f_{oc}$ approach, with use of measured K_{oc} values (Brusseau, 2019).
209 Measured values for K_{aw} were taken from Brusseau and Van Glubt (2021). Values for a_{aw} were
210 estimated using measured data reported for several porous media comprising a range of textures
211 (Peng and Brusseau, 2005; Brusseau and Guo, 2021; El Ouni et al., 2021).

212 The fourth component of the study comprises two sets of numerical simulations for a
213 model fire-training source area. The first set focuses on the long-term distribution of PFAS in the
214 vadose zone and the magnitudes of soil versus porewater concentrations for representative field
215 conditions, while the second set illustrates the impact of a precipitation event on short-term
216 changes in $\frac{C_t}{C_p}$. The mathematical model that was employed to conduct the numerical simulations
217 accounts for transient variably saturated flow, surfactant-induced flow, nonlinear and rate-limited
218 solid-phase sorption, and nonlinear and rate-limited air-water interfacial adsorption (Guo et al.,
219 2020). A 30-year period of operation is used wherein PFAS are released to the vadose zone due
220 to regular fire training activities. This is followed by a post-operation period where the release of
221 PFAS is stopped. The measured properties for a well-characterized soil (Vinton) are used to
222 represent a homogeneous vadose zone.

223 Three representative PFAS (PFPeA, PFOA, and PFOS) are considered. The PFAS are
224 released to the vadose zone in a 1% diluted AFFF solution at concentrations of 0.23 mg/L, 0.9
225 mg/L, and 100 mg/L, respectively, for PFPeA, PFOA, and PFOS. Real rainfall and evaporation
226 data at 30-min resolution from a site in New Jersey are used to represent the climatic conditions
227 for a humid region. The details of the model setup and other input parameters are the same as
228 those used in the numerical simulations reported in Guo et al (2022). The analysis in the present

study focuses on the post-operation period. In addition to the long-term numerical simulations, a set of short-term (10 day) simulations is conducted to analyze the dynamic changes of porewater concentration and the ratio of total to porewater concentration during and immediately after a relatively large storm. The PFAS concentration at the end of the 30-year contamination period is used as the initial condition for these short-term simulations.

4. Results and Discussion

4.1 The C_t versus C_p relationship as a function of PFAS, soil properties, and water saturation

Inspection of equation 8 reveals that relative distribution of PFAS between the different domains within a soil sample, represented by R_d, is a function of both properties of the PFAS and properties of the soil. It has been demonstrated that both K_d and K_{aw} are functions of the molecular size of PFAS (e.g., Higgins and Luthy, 2006; Brusseau, 2019a, 2019b). The magnitude of sorption will also be a function of the geochemical properties of the soil, such as the constituent contents and compositions (e.g., organic carbon, clay minerals, metal oxides). The magnitude of air-water interfacial adsorption will be mediated by the amount of air-water interface present, which is a function in part of soil properties (grain size, solid surface area). Finally, it is observed that R_d is a function water content for a given soil and PFAS, both directly through the θ_w terms and indirectly through the dependence of a_{aw} on water content. It is well established that a_{aw} increases with decreasing θ_w (e.g., Kim et al., 1997; Anwar et al., 2000; Peng and Brusseau, 2005; Brusseau and Guo, 2021; El Ouni et al., 2021). As a result of these functionalities for R_d, the ratio between C_t and C_p is a function of PFAS molecular size, soil properties, and water content. These dependencies are illustrated in this section.

The C_t/C_p relationship as a function of water saturation is presented in Figure 1 for the four selected PFAS. C_t/C_p is observed to be less than one for PFBA and PFOA over the entire range of water saturation. Inspection of equation 7 reveals that for sufficiently small R_d values, C_t/C_p will be less than one due to the impact of the $\frac{\theta_w}{\rho_b}$ term (which is always <1). The C_t/C_p decreases with decreasing water saturation for PFBA. This is due to the minimal impact of air-water interfacial adsorption on PFBA distribution within the sample. As a result, the increase in R_d that results from decreasing water saturation is less than the corresponding decrease in the $\frac{\theta_w}{\rho_b}$ term. Conversely, the C_t/C_p increases with decreasing water saturation for PFOA. This is due to a substantial increase in R_d accruing to the impact of air-water interfacial adsorption and the increase in the magnitude of air-water interfacial area with decreasing water saturation.

In contrast to PFBA and PFOA, the C_t/C_p values for PFTDA and PFOS are >1 for all and almost all water saturations, respectively. This is a result of the larger magnitudes of solid-phase sorption for PFOS and particularly PFTDA (see respective K_d values in Table 1). C_t/C_p increases with decreasing water saturation for PFTDA and PFOS due to the impact of air-water interfacial adsorption as described above for PFOA.

The C_t/C_p relationship for PFOS as a function of water saturation is presented in Figure 2 for three porous media. The C_t/C_p values are largest for the Vinton soil at any given water saturation because this medium has the largest magnitude of air-water interfacial area (Table 2). Conversely, the C_t/C_p values are smallest for the sand due to the smaller K_d and a_{aw} values.

The specific impact of air-water interfacial adsorption, and the underlying influence of the decrease in water saturation on the relative significance of this process, is illustrated by comparing the PFOS C_t/C_p values for the cases with and without air-water interfacial adsorption in Figures 1 and 2. The divergence between the paired sets of curves progressively increases as

274 water saturation decreases in all cases. Similar results are observed for PFTDA (data not shown).
275 These results highlight the impact of air-water interfacial adsorption on the distribution of
276 longer-chain PFAS within soil samples. This retention process will significantly influence
277 porewater concentrations under certain conditions.

278 ***4.2 Prediction of measured soil-to-porewater concentration ratios***

279 The outdoor lysimeter study of Felizeter et al. (2021) represents one of the first to present
280 field-based measurements of PFAS porewater concentrations. The measured porewater
281 concentrations range from 0.1 to ~4000 µg/L depending upon the individual PFAS (Table 3).
282 The measured soil concentrations (C_s) range from ~0.3 to ~8000 µg/kg. The measured soil
283 concentrations are designated as C_s to differentiate them from the theoretical C_t term, as will be
284 discussed in more detail in section 4.5.

285 The measured C_s and C_p data reported in the study were used to determine measured
286 C_s/C_p values. Inspection of Table 3 shows that the measured C_s/C_p values are <1 for the shortest-
287 chain PFAS and >1 for the longer-chain PFAS, consistent with the results presented in Figure 1.
288 This again is due to the different magnitudes of retention experienced by the short-chain versus
289 long-chain PFAS under the extant conditions of the experiment. Measured R_d values were
290 calculated with equation 7 using the measured C_s/C_p values, and are presented in Table 3. The
291 measured R_d values range by more than three orders of magnitude, from 1 for PFBA to 1777 for
292 PFTDA. The values are observed to be a function of PFAS size. This is illustrated by Figure 3,
293 wherein log R_d is shown to be a linear function of PFAS molar volume. This is consistent with
294 prior research demonstrating that both log K_d and Log K_{aw} for PFAS are functions of molar
295 volume (Brusseau, 2019a, 2019b).

296 Predicted C_t/C_p values were produced with the distribution model using equation 7. This
297 was accomplished with the use of independently-obtained parameters to determine R_d for each
298 PFAS with equation 8. The predicted C_t/C_p values are compared to the measured C_s/C_p values in
299 Figure 4 for two cases, one incorporating air-water interfacial adsorption and one without. The
300 predicted values that incorporate air-water interfacial adsorption match very well to the measured
301 values for all PFAS except PFBS. The excellent predictions of the measured data indicate that
302 the model provides a reasonable representation of PFAS mass distribution within the soil
303 samples. The importance of air-water interfacial adsorption for the longer-chain PFAS is
304 illustrated by the significant differences in the predicted values for the two cases with and
305 without air-water interfacial adsorption.
306 In considering the deviation between predicted and measured values observed for PFBS,
307 it is critical to note that air-water interfacial adsorption is predicted to have minimal impact on
308 PFBS distribution for this soil. Hence, the deviation may be due in part to an inaccurate
309 representation of solid-phase sorption (inaccurate K_d). In addition, the measured values for all
310 PFAS exhibit a degree of variability. This is related in part to variability in the water contents of
311 the individual treatments, which ranged from 0.20 to 0.27, and inherent experimental
312 uncertainty.
313
314 ***4.3 The C_t versus C_p relationship under dynamic short-term and long-term field conditions***
315 The predicted C_t and C_p values, along with the $\frac{C_t}{C_p}$ relationships, simulated for long-term
316 field conditions at a model fire training area site are presented in Figure 5. The total soil
317 concentrations after the 30 years of site operation are observed to range from approximately 1
318 µg/kg for PFPeA to ~50 µg/kg for PFOA to ~25 mg/kg for PFOS (Figure 5). These

319 concentrations are consistent with PFAS soil-concentration ranges observed at AFFF-impacted
320 sites (Brusseau et al., 2020). The porewater concentrations after the 30 years of operation range
321 from approximately 5 µg/L for PFPeA to 18 µg/L for PFOA to 1300 µg/L for PFOS. These are
322 consistent with porewater concentrations reported at AFFF-impacted sites (Davis et al. 2021;
323 Quinnan et al., 2021). Both PFPeA and PFOA have migrated to the bottom of the simulated
324 vadose zone within the 30 year operation period. Conversely, the PFOS front has migrated to
325 only a 250-cm depth in this timeframe due to its significantly greater retention. The C_t and C_p
326 values for all three PFAS decrease over the post-operation period due to leaching. The
327 downward migration of the contaminant plume is clearly observed for PFOS, with the peaks of
328 both C_t and C_p migrating to successively greater depths over the 50-year post-operation period.
329 The C_t/C_p values vary greatly among the three PFAS—the ratio for PFOS is almost 10
330 and 100 times those for PFOA and PFPeA, respectively (Figure 5). Consistent with Equation 8,
331 the variation is caused primarily by the differences in the relative magnitudes of retention due to
332 solid-phase sorption and air-water interfacial adsorption. Inspection of Figure 5 shows that the
333 C_t/C_p changes in space and time for each PFAS. The changes are driven by spatial and temporal
334 changes in concentration due to the migration of the plume, and accompanying changes in the
335 magnitudes of retention related to nonlinearity of solid-phase sorption and/or air-water interfacial
336 adsorption. The water content changes minimally over time for these long-term simulations (data
337 not shown), and therefore does not measurably impact the observed results.
338 The C_t/C_p increases with time throughout the depth profile for PFPeA and PFOA, and for
339 the upper ~120 cm for PFOS. This results from the temporal decrease in porewater
340 concentrations and the resultant increase in the magnitude of sorption and/or air-water interfacial
341 adsorption. For PFPeA and PFOA, the porewater concentrations are several orders of magnitude

342 below the concentrations at which air-water interfacial adsorption becomes essentially linear.
343 Thus, the change in C_t/C_p is primarily due to nonlinearity of solid-phase sorption. Conversely,
344 the porewater concentration for PFOS is much higher and the changes in C_t/C_p are caused
345 primarily by nonlinear air-water interfacial adsorption. The PFOS C_t/C_p decreases over time in
346 the deeper interval, reflecting the increase in concentration as the solute front migrates into this
347 interval. The C_t/C_p goes to zero for PFOS in the bottom region of the domain. This occurs where
348 the total and porewater concentrations are zero because the plume has not yet entered that depth
349 interval. This is observed only for PFOS because it has much greater retention than PFOA and
350 PFPeA, and therefore the PFOS front has not yet migrated to the bottom of the interval as noted
351 above.

352 The short-term simulations (Figure 6) clearly show that different magnitudes of change
353 occur for soil and porewater concentrations for the different PFAS. Significant changes in total
354 soil concentrations are observed for PFPeA during the simulated 10-day storm event.
355 Conversely, there is minimal change in C_t for PFOA and PFOS. This disparity reflects a greater
356 amount of leaching affecting PFPeA due to its significantly lower retention in comparison to
357 PFOA and especially PFOS. In contrast to the relative changes in C_t, the greatest changes in
358 porewater concentrations are observed for PFOS and PFOA whereas minimal changes are
359 observed for PFPeA. As a result, the C_t/C_p varies significantly for the former two, up to 50% for
360 PFOA and up to ~5 times for PFOS, and minimally for PFPeA.

361 The changes observed for C_p and C_t/C_p are caused by changes in the local water
362 saturation during the infiltration/redistribution event and the subsequent changes in air-water
363 interfacial area caused by these transient water-content conditions (Figure 7). Inspection of
364 Figure 7 shows that the increased water saturation due to the wetting front infiltration destroys

365 air-water interfacial area. As a result, the PFAS adsorbed at the air-water interfaces are
366 subsequently released to the porewater, causing an increase in the porewater concentration.
367 Large changes in C_p and C_t/C_p are observed for PFOA and PFOS because air-water interfacial
368 adsorption provides a significant contribution to total retention. Smaller changes are observed for
369 PFPeA because air-water interfacial adsorption provides a much smaller contribution to total
370 retention. These dynamic changes of porewater concentration due to transient water infiltration
371 are consistent with those reported in our prior work (Guo et al., 2020; Zeng et al., 2021). The
372 transient changes in porewater concentration and the C_t/C_p have important implications for
373 designing and operating porewater sampling lysimeters.
374
375 ***4.4 Field measured soil versus porewater concentrations***
376 One of the first full-scale field applications of direct soil porewater sampling for PFAS
377 was reported by Quinnan et al. (2021). This study comprised a test of high-resolution site
378 characterization methods for quantifying PFAS concentrations and mass discharge for an
379 aqueous film-forming foam (AFFF) source area at an Army Airfield facility. Three sampling
380 lysimeters were installed in the vadose zone of the source area. The area was irrigated prior to
381 porewater sample collection to facilitate sample collection. The sections within which each of the
382 lysimeters resided received different magnitudes and rates of irrigation. Soil samples were
383 collected from the intervals in which the lysimeters were installed to provide paired sample sets.
384 The samples were analyzed for 13 PFAS, including PFOS and PFOA. This discussion will focus
385 on the results presented for lysimeter LS-3R and the associated soil samples, which was in the
386 section that received the lowest rate of irrigation.

387 The highest PFAS soil concentrations were reported for PFOS, which was ~300 µg/kg
388 for the selected section. In comparison, concentrations of 1.8, 1.5, and 1.2 µg/kg were reported
389 for PFNA, PFOA, and PFHxS, respectively, for the same section. The highest PFAS
390 concentrations in soil porewater were also reported for PFOS, 6 µg/L for the selected lysimeter.
391 Concentrations of 0.3, 1, and 1.1 µg/L were reported for PFNA, PFOA, and PFHxS,
392 respectively. Values for C_s/C_p were calculated using the reported concentration pairs. The values
393 range from 51 for PFOS, 6 for PFNA, to values of 1-2 for the shorter-chain PFAS (PFOA,
394 PFHpA, PFHxA, PFPeA, PFHxS, PFHxA). The ratios are observed to be larger for the longer-
395 chain PFAS and smaller for the shorter-chain PFAS, which is consistent with the analyses
396 presented above.
397
398 ***4.5 Practical implications***
399 There are multiple implications to the results of this study. One aspect is the relationship
400 between soil concentrations and total concentrations. If the soil sample is collected in a manner
401 that retains all PFAS mass, then C_s would be equivalent to C_t. Conversely, C_s would be
402 anticipated to be lower than C_t if some fraction of mass is lost during sample collection and
403 processing. Generally, for PFAS with low vapor-pressures, the primary potential source of mass
404 loss may be anticipated to occur via partial drainage of porewater during sample collection and
405 processing. From equations 4 and 8, $1/R_d$ represents the fraction of PFAS mass present in
406 porewater. For R_d >20, the mass present in porewater represents <5% of the total mass. Hence, it
407 is observed that the loss of some portion of porewater during sample collection and processing
408 will not significantly influence the representativeness of the soil concentrations for samples for
409 which R_d values are relatively large. However, measured C_s values will not be fully

410 representative of C_t when porewater loss occurs for conditions with smaller R_d values. The issue
411 of PFAS recovery during sample processing is a separate issue that can of course affect actual C_s
412 values measured.

413 The distribution model presented herein can be used to examine the anticipated range of
414 concentrations of PFAS in porewater, based on measured soil concentrations. Brusseau et al.
415 (2020) conducted a meta-analysis of measured PFAS soil concentrations and observed
416 concentrations ranged over many orders of magnitude, depending in part on the type of site. For
417 example, soil concentrations up to 100s of mg/kg have been reported for AFFF-impacted sites.
418 Hence, the associated porewater concentrations for these sites can be anticipated to be in the
419 range of µg/L to mg/L depending upon the specific PFAS and the soil properties and conditions.

420 Guo et al. (2020) conducted long-term numerical simulations for a model fire-training
421 source area for representative field conditions. Porewater concentrations ranging up to 10's of
422 mg/L were obtained for PFOS, for a simulated release concentration of 1,000 mg/L. The
423 simulations presented in section 4.3 produced porewater concentrations ranging up to ~1 mg/L
424 for a simulated release concentration of 100 mg/L. As noted in the preceding section, Quinnan et
425 al. (2021) reported porewater concentrations for PFOS ranging up to 6 µg/L for an AFFF-
426 impacted site. Davis et al. (2021) reported a porewater concentration of ~16 mg/L for total PFAS
427 for an AFFF-impacted site. These results are consistent with the concentrations anticipated for
428 sites with relatively high soil concentrations.

429 In contrast to primary-source sites that typically have relatively high soil concentrations,
430 PFAS porewater concentrations are anticipated to be significantly lower for secondary-source
431 sites such as locations receiving land application of biosolids or treated wastewater. Porewater
432 concentrations are anticipated to be lower still for sites for which no known PFAS sources are

433 nearby. For example, the median of maximum reported PFOS soil concentrations was 2.7 µg/kg
434 for sites with no known nearby PFAS sources (Brusseau et al., 2020). Porewater concentrations
435 are anticipated to be in the ng/L to lower µg/L range for such sites. Discussion of relevant
436 porewater concentrations for transport investigations and risk assessments need to account for
437 these anticipated ranges in concentrations.
438
439 **5. Conclusion**
440 The objective of this research was to delineate the relationship between soil porewater
441 concentrations and soil concentrations, based on a comprehensive model of PFAS mass
442 distribution within a soil sample volume. The distribution model was used to illustrate the impact
443 of PFAS chain length and soil properties on the ratio of soil concentration to soil porewater
444 concentration. For a given soil, the ratio is greater for longer-chain PFAS. And, for a given
445 PFAS, it is larger for soils with greater sorption capacities and larger air-water interfacial areas.
446 For a given soil and PFAS for which air-water interfacial adsorption is important, the ratio
447 increases with decreasing water content due to the increase in air-water interfacial area.
448 Measured data reported in the literature for soil and soil porewater concentrations of
449 several PFAS obtained from outdoor lysimeter experiments were used to test the distribution
450 model. Soil-to-porewater concentration ratios predicted with the model compared very well to
451 the measured concentration ratios. The nondimensional distribution coefficient that describes the
452 distribution of PFAS mass among all domains within a soil sample was observed to be a function
453 of PFAS molecular size. Numerical simulations conducted for a model fire-training source area
454 were used to illustrate the magnitudes of soil versus porewater concentrations for representative
455 field conditions. The results of the measured and simulated data sets demonstrated the

456 importance of air-water interfacial adsorption for the distribution of the longer-chain PFAS
457 within soil samples. This work has demonstrated the relationship between porewater
458 concentrations and soil concentrations and the factors that influence the distribution of PFAS
459 within a soil sample. Soil concentrations are what are typically reported for site investigations.
460 However, porewater concentrations represent the mass that is directly subject to migration and
461 mass discharge to groundwater. In addition, porewater concentrations generally comprise what is
462 readily bioavailable to plant roots and soil microorganisms. Thus, the importance of
463 understanding this relationship is evident. PFAS soil porewater concentrations are anticipated to
464 range from ng/L to mg/L depending on soil concentrations, which in turn depend on the nature of
465 the site. These ranges in concentrations need to be accounted for in discussions of relevant
466 porewater concentrations for transport and fate investigations and risk assessments. The
467 distribution model presented herein is anticipated to be useful for developing and enhancing
468 conceptual site models and for conducting site investigations, risk assessments, and remediation-
469 feasibility studies.
470

471 **Acknowledgements**

472 This research was supported by the Superfund Research Program of the NIEHS (P42 ES 4940),
473 the Hydrologic Sciences Program of the NSF (2023351), and the Environmental Security
474 Technology Certification Program (Project ER21–5041). We thank the reviewers for their
475 constructive comments.
476

477 **References**

478 Anderson, R.H.. 2021. The case for direct measures of soil-to-groundwater contaminant mass
479 discharge at AFFF-impacted sites. Environ. Sci. Technol. 2021, 55, 6580-6583.

480
481 Anderson, R.H., Adamson, D.T., Stroo, H.F., 2019. Partitioning of poly-and perfluoroalkyl
482 substances from soil to groundwater within aqueous film-forming foam source zones. J. Contam.
483 Hydrol. 220, 59-65.
484
485 Anwar, A.H.M.F., Bettahar, M., Matsubayashi, U., 2000. A method for determining airwater
486 interfacial area in variably saturated porous media. J. Contam. Hydrol. 43, 129–146.
487
488 Baduel, C., Mueller, J. F., Rotander, A., Corfield, J., and Gomez-Ramos, M. J., 2017. Discovery
489 of Novel Per and Polyfluoroalkyl Substances (PFASs) at a Fire Fighting Training Ground and
490 Preliminary Investigation of Their Fate and Mobility. Chemosphere, 185, 1030–1038.
491
492 Brusseau, M.L., 2018. Assessing the potential contributions of additional retention processes to
493 PFAS retardation in the subsurface. Sci. Total Environ. 613-614,176-185.
494
495 Brusseau, M. L., 2019a. The influence of molecular structure on the adsorption of PFAS to fluid-
496 fluid interfaces: Using QSPR to predict interfacial adsorption coefficients. Water Res. 152, 148-
497 158.
498
499 Brusseau, M. L., 2019b. Estimating the relative magnitudes of adsorption to solid-water and
500 air/oil-water interfaces for per- and poly-fluoroalkyl substances. Environ. Pollut. 254, article
501 113102.
502
503 Brusseau, M. L. and Guo, B., 2021. Air-water interfacial areas relevant for transport of per and
504 poly-fluoroalkyl substances. Water Res., 207, 117785.
505
506 Brusseau, M. L. and Van Glubt, S., 2021. The influence of molecular structure on PFAS
507 adsorption at air-water interfaces in electrolyte solutions. Chemosphere 281, 130829.
508

509 Brusseau, M. L., Yan, N., Van Glubt, S., Wang, Y., Chen, W., Lyu, Y., Dungan, B., Carroll, K.
510 C., Holguin, F. O., 2019a. Comprehensive retention model for PFAS transport in subsurface
511 systems. Water Res. 148, 41-50.
512
513 Brusseau, M. L., Khan, N., Wang, Y. K., Yan, N., Van Glubt, S., Carroll, K. C., 2019b. Nonideal
514 transport and extended elution tailing of PFOS in soil. Environ. Sci. Technol. 53, 10654-10664.
515
516 Brusseau, M. L., Anderson, R. H., Guo, B., 2020. PFAS concentrations in soils: Background
517 levels versus contaminated sites. Sci. Total Environ. 740, article 140017.
518
519 Brusseau, M.L., Guo, B., Huang, D., Yan, N. and Lyu, Y., 2021. Ideal versus nonideal transport
520 of PFAS in unsaturated porous media. Water Research, 202, article 117405.
521
522 Dauchy, X., Boiteux, V., Colin, A., Hémard, J., Bach, C., Rosin, C.,Munoz, J., 2019. Deep
523 seepage of per- and polyfluoroalkyl substances through the soil of a firefighter training site and
524 subsequent groundwater contamination. Chemosphere 214, 729–737.
525
526 Davis, K., Aucoin, M., Larsen, B., Kaiser, M., & Hartten, A., 2007. Transport of ammonium
527 perfluorooctanoate in environmental media near a fluoropolymer manufacturing facility.
528 Chemosphere, 67(10), 2011-2019.
529
530 Davis, G. B., Wallis, I., Kookana, R., Navarro, D., Rayner, J. L., and Prommer, H., 2021. Key
531 unsaturated zone soil processes for PFAS mobility and retention: principles and understanding.
532 CSIRO, Australia. Report for the PFAS Investigation & Management Branch, Department of
533 Defence.
534
535 El Ouni, A., Guo, B., Zhong, H., Brusseau, M.L., 2021. Testing the validity of the miscible-
536 displacement interfacial tracer method for measuring air–water interfacial area: Independent
537 benchmarking and mathematical modeling. Chemosphere 263, Article
538 128193.
539

Felizeter, S., H. Jürling, M. Kotthoff, P. De Voogt, and M.S. McLachlan, 2021. Uptake of perfluorinated alkyl acids by crops: Results from a field study. Environ. Sci. Proc. Impacts, 23, 1158.

Filipovic, M., Woldegiorgis, A., Norström, K., Bibi, M., Lindberg, M., Österås, A., 2015. Historical usage of aqueous film forming foam: a case study of the widespread distribution of perfluoroalkyl acids from a military airport to groundwater, lakes, soils and fish. Chemosphere 129, 39–45.

Gellrich, V., Stahl, T., and Knepper, T.P. 2012. Behavior of perfluorinated compounds in soils during leaching experiments. Chemosphere, 87, 1052−1056.

Guelfo, J.L.,Wunsch, A., Mccray, J., Stults, J.F., Higgins, C.P., 2020. Subsurface transport potential of perfluoroalkyl acids (PFAAs): column experiments and modeling. J. Contam. Hydrol., 233, 9–20.

Guo, B., Zeng, J., Brusseau, M.L., 2020. A Mathematical Model for the Release, Transport, and Retention of Per- and Polyfluoroalkyl Substances (PFAS) in the Vadose Zone. Water Resour. Res. 56 (2), 21.

Guo, B., Zeng, J., Brusseau, M.L. and Zhang, Y., 2022. A screening model for quantifying PFAS leaching in the vadose zone and mass discharge to groundwater. Advances in Water Resources. Article 104102.

Higgins C.P., R. G. Luthy, 2006. Sorption of perfluorinated surfactants on sediments. Environ. Sci. Technol. 40 (23), 7251-6.

Høisæter, Å., Pfaff, A., Breedveld, G.D., 2019. Leaching and transport of PFAS from aqueous film-forming foam (AFFF) in the unsaturated soil at a firefighting training facility under cold climatic conditions. J. Contam. Hydrol. 222, 112–122.

570 Johnson, G.R., 2022. PFAS in soil and groundwater following historical land application of
571 biosolids. Water Research, 211, Article 118035.
572
573 Kim, H., Rao, P.S.C., Annable, M.D., 1997. Determination of effective air-water interfacial area
574 in partially saturated porous media using surfactant adsorption. Water Resour. Res. 33 (12),
575 2705–2711.
576
577 Lyu, Y., Brusseau, M., Chen, W., Yan, N., Fu, X., Lin, X., 2018. Adsorption of PFOA at the
578 air-water Interface during transport in unsaturated porous media. Environ. Sci. Technol. 52,
579 7745–7753.
580
581 McLachlan, M.S., S. Felizeter, M. Klein, M. Kotthoff, and P. Voogt. 2019. Fate of a
582 perfluoroalkyl acid mixture in an agricultural soil studied in lysimeters, Chemosphere, 223, 180–
583 187.
584
585 Milinovic, J., Lacorte, S., Vidal, M., Rigol, A., 2015. Sorption behaviour of perfluoroalkyl
586 substances in soils. Sci. Total Environ. 511, 63-71.
587
588 Nickerson, A., Rodowa, A.E., Adamson, D.T., Field, J.A., Kulkarni, P.R., Kornuc, J.J. and
589 Higgins, C.P., 2021. Spatial trends of anionic, zwitterionic, and cationic PFASs at an AFFF-
590 impacted site. Environ. Sci. Technol., 55, 313-323.
591
592 Peng, S. and Brusseau, M.L., 2005. Impact of soil texture on air-water interfacial areas in
593 unsaturated sandy porous media. Water Resour. Res. 41, Article W03021.
594
595 Pepper, I,L., M.L. Brusseau, F.J. Prevatt, and B.A. Escobar. Incidence of PFAS in soil following
596 long-term application of class B biosolids. Sci. Total Environ., 793, Article 148449.
597
598 Quinnan, J., Rossi, M., Curry, P., Lupo, M., Miller, M., Korb, H., Orth, C., Hasbrouck, K., 2021.
599 Application of PFAS- mobile lab to support adaptive characterization and flux- based conceptual
600 site models at AFFF releases. Remediation, 31, 7–26.

Quinnan, J., Curry, P., Lupo, M., Miller, M., Rossi, M., 2021. Validation of Streamlined Mobile Lab-Based Real Time PFAS Analytical Methods. Final Report ESTCP Project ER19-5203, May 2021.

Sepulvado, J., Blaine, A., Hundal, L., & Higgins, C., 2011. Occurrence and fate of perfluorochemicals in soil following the land application of municipal biosolids. Environ. Sci. Technol., 45, 8106-8112.

Silva, J.A.K., Simůnek, J., and McCray, J.E., 2020. A modified HYDRUS model for simulating PFAS transport in the vadose zone. Water 12, 2758.

Van Glubt, S., Brusseau, M. L., Yan, N., Huang, D. D., Khan, N. & Carroll, K. C., 2021. Column versus Batch Methods for Measuring PFOS and PFOA Sorption to Geomedia. Environ. Pollut. 268, 115917.

Vierke, L., A. Möller, and Ss Klitzke. 2014. Transport of perfluoroalkyl acids in a water-saturated sediment column investigated under near-natural conditions. Environ. Poll. 186, 7-13.

Washington, J., Yoo, H., Ellington, J., Jenkins, T., & Libelo, E., 2010. Concentrations, distribution, and persistence of perfluoroalkylates in sludge-applied soils near Decatur, Alabama, USA. Environ. Sci. Technol., 44(22), 8390-8396.

Weber, A.K., Barber, L.B., LeBlanc, D.R., Sunderland, E.M., Vecitis, C.D., 2017. Geochemical and hydrologic factors controlling subsurface transport of polyand perfluoroalkyl substances, Cape Cod, Massachusetts. Environ. Sci. Technol. 51, 4269-4279.

Xiao, F., Simcik, M.F., Halbach, T.R., Gulliver, J.S., 2015. Perfluorooctane sulfonate (PFOS) and perfluorooctanoate (PFOA) in soils and groundwater of a U.S. metropolitan area: migration and implications for human exposure. Water Res. 72, 64-74.

Zeng, J., Brusseau, M.L. and Guo, B., 2021. Model validation and analyses of parameter sensitivity and uncertainty for modeling long-term retention and leaching of PFAS in the vadose zone. J. Hydrology, 603, p.127172.

Tables

Table 1. PFAS Parameter Values

PFAS	**K_{aw}** (cm)	**K_d-Sand** (cm^3/g)	**K_d-Eustis** (cm^3/g)	**K_d-Vinton** (cm^3/g)	**K_d-Soil**[a] (cm^3/g)
PFBA	0.00003	0.07	-	-	0.03
PFHxA	0.0002	-	-	-	0.19
PFOA	0.003	0.15	-	-	1.0
PFNA	0.014	-	-	-	2.5
PFDA	0.07	-	-	-	7.9
PFUnDA	0.128	-	-	-	28
PFTrDA	0.26	2.8	-	-	154
PFBS	0.00017	-	-	-	0.12
PFOS	0.05	0.25	1.9	1.9	5.7
Data Source	Brusseau & Van Glubt, 2021	Van Glubt et al., 2021	Brusseau et al., 2019b	Brusseau et al., 2019b	Brusseau, 2019b

[a]Medium for the Felizeter et al. (2021) study

Table 2. Air-Water Interfacial Area Values

Porous Medium	**Range of S_w Values**[b]	**Range of a_{aw} Values**[c] (cm^{-1})
Sand	0.2-1	0-419
Eustis	0.2-1	0-656
Vinton	0.2-1	0-1026
Soil[a]	0.51-0.68	428-866

[a]Medium for the Felizeter et al. (2021) study

[b]S_w is water saturation

[c]Air-water interfacial area is a function of water saturation

Table 3. Porewater Data from the Felizeter et al. (2021) Study

PFAS	**C_p (ug/L)**	**R_d Measured[a]**
PFBA	36-225	1.0
PFHxA	0.4-127	3.2
PFOA	3-3994	11.6
PFNA	0.2-1777	52.7
PFDA	0.1-293	248
PFUnDA	42-6000	702
PFTDA	5-81	1785
PFBS	3-175	7.4
PFOS	3-548	195

[a]Calculated for this study using the raw data reported in Felizeter et al. (2021)

Figure Captions

Figure 1. Ratio of total soil concentration (C_t) to porewater concentration (C_p) of an individual PFAS for four representative PFAS. Parameters used are representative of the sand. AWIA represents air-water interfacial adsorption.

Figure 2. Ratio of total soil concentration (C_t) to porewater concentration (C_p) for PFOS in three porous media. AWIA represents air-water interfacial adsorption.

Figure 3. Measured nondimensional distribution coefficients, R_d, as a function of PFAS molar volume. Measured values determined from raw data reported in Felizeter et al., (2021).

Figure 4. Comparison of predicted and measured porewater concentrations for several PFAS (Table 3). Measured data determined from raw data reported in Felizeter et al., (2021). AWIA represents air-water interfacial adsorption. The error bars represent 95% confidence intervals. The one outlier data point (red circle) is PFBS.

Figure 5. Ratio of total soil concentration (Ct) to porewater concentration (Cp) (left column), Cp (center column), and Ct (right column) from the long-term simulations of PFAS leaching in a model fire training area site during the post contamination period (i.e., after fire training activities stopped). The three rows denote the results for PFPeA, PFOA, and PFOS, respectively.

Figure 6. Ratio of total soil concentration (Ct) to porewater concentration (Cp) (left column), Cp (center column), and Ct (right column) from the short-term simulations of PFAS leaching in a model fire training area site. Simulated PFAS concentration in the vadose zone at the end of the contamination period is used as the initial conditions and no PFAS were released to the vadose zone during the simulations. The simulated 60-day period contains one of the largest rainfall events over a period of ten years. The three rows denote the results for PFPeA, PFOA, and PFOS, respectively.

Figure 7. Spatial profiles of water saturation and specific air-water interfacial area during the 10-day period of short-term simulations. The results for the PFPeA simulations are presented here, but the water saturation and air-water interfacial area for the PFOA and PFOS simulations are almost the same as surfactant-induced flow has a relatively minor impact.

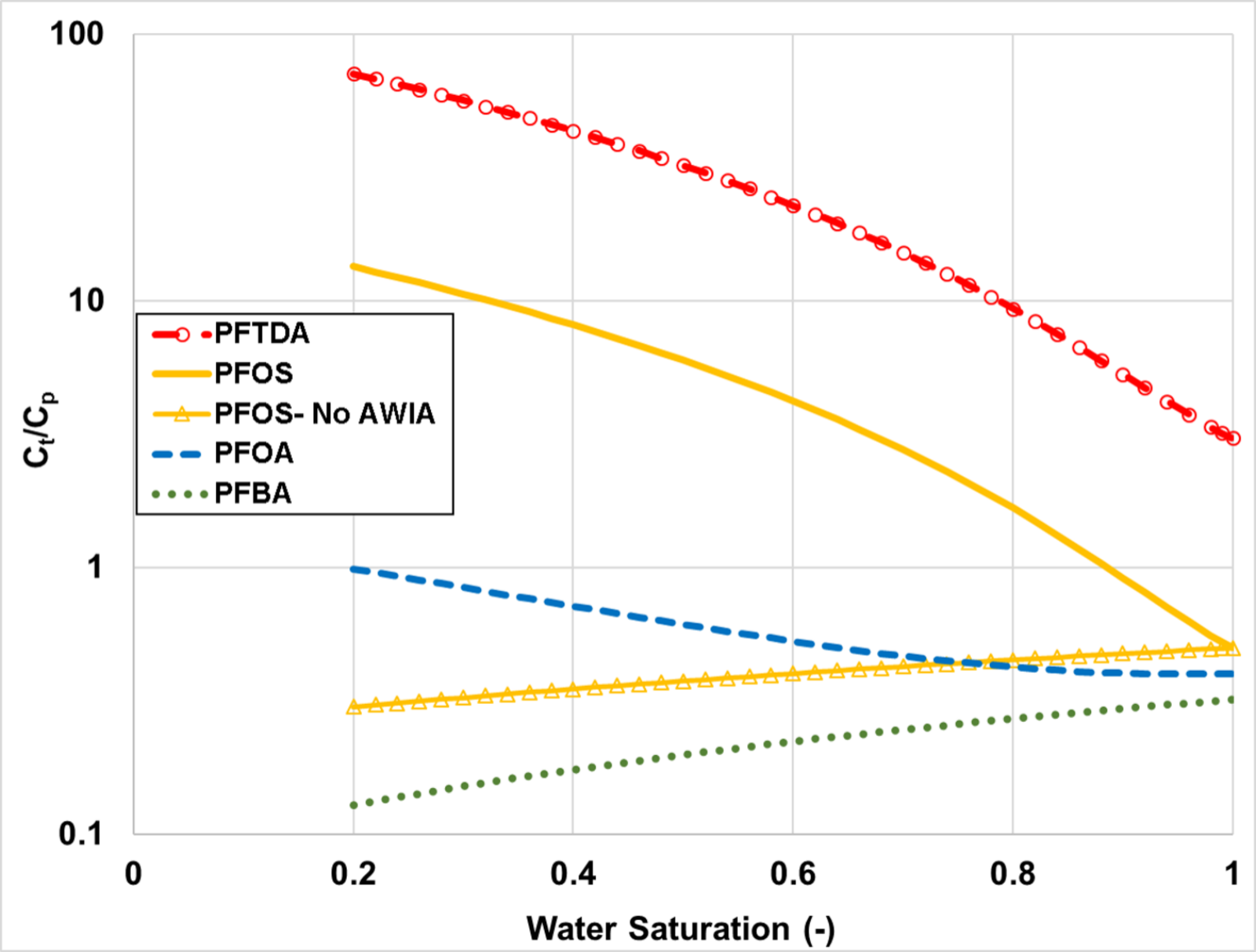
100
10
1
0.1
C_t/C_p
PFTDA
PFOS
PFOS- No AWIA
PFOA
PFBA
0
0.2
0.4
0.6
0.8
1
Water Saturation (-)

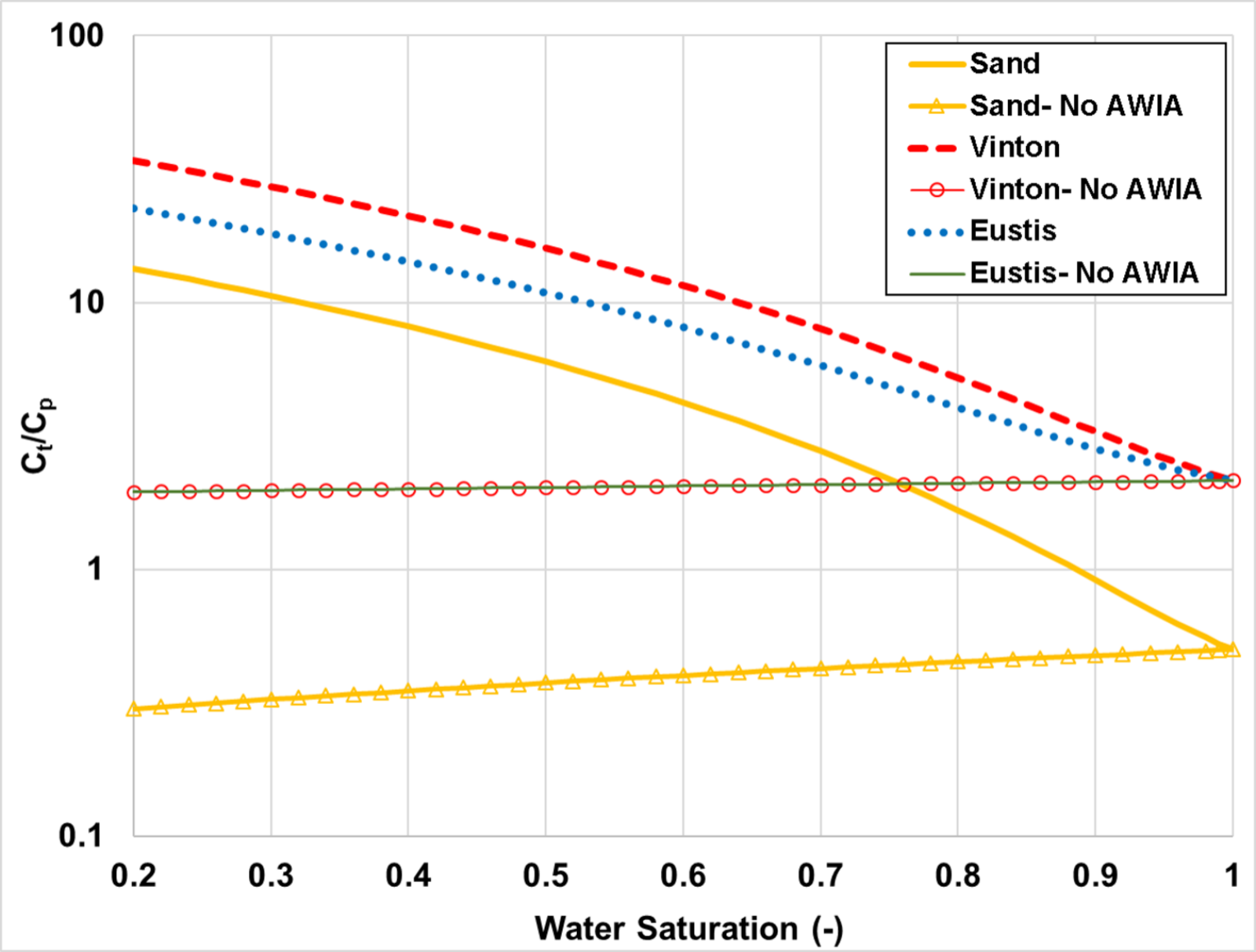
100
10
1
0.1
C_t/C_p
0.2
0.3
0.4
0.5
0.6
0.7
0.8
0.9
1
Water Saturation (-)
Sand
Sand- No AWIA
Vinton
Vinton- No AWIA
Eustis
Eustis- No AWIA

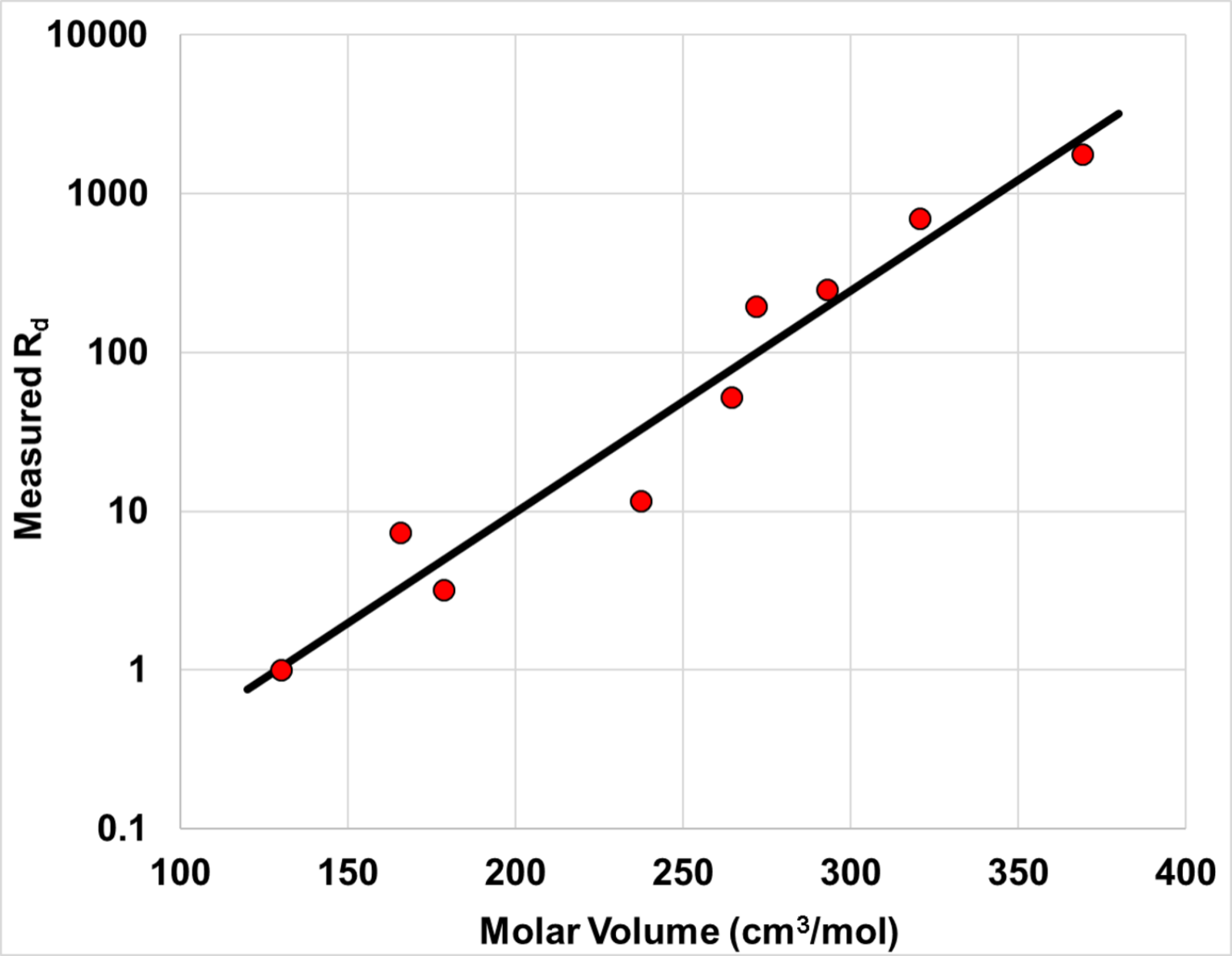
10000
1000
100
10
1
0.1
Measured R_d
100
150
200
250
300
350
400
Molar Volume (cm^3/mol)

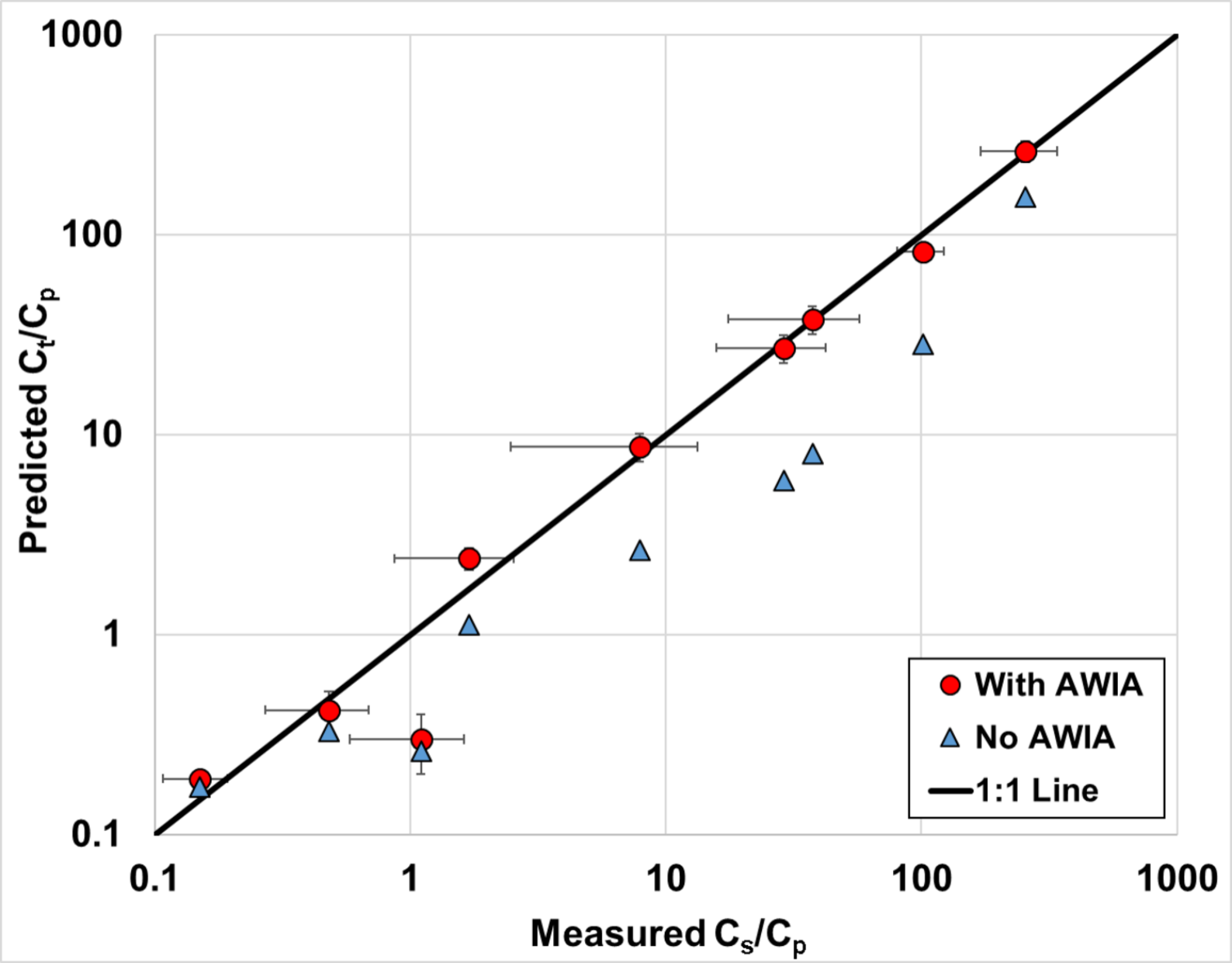
1000
100
10
1
0.1
Predicted C_t/C_p
0.1
1
10
100
1000
Measured C_s/C_p
With AWIA
No AWIA
1:1 Line

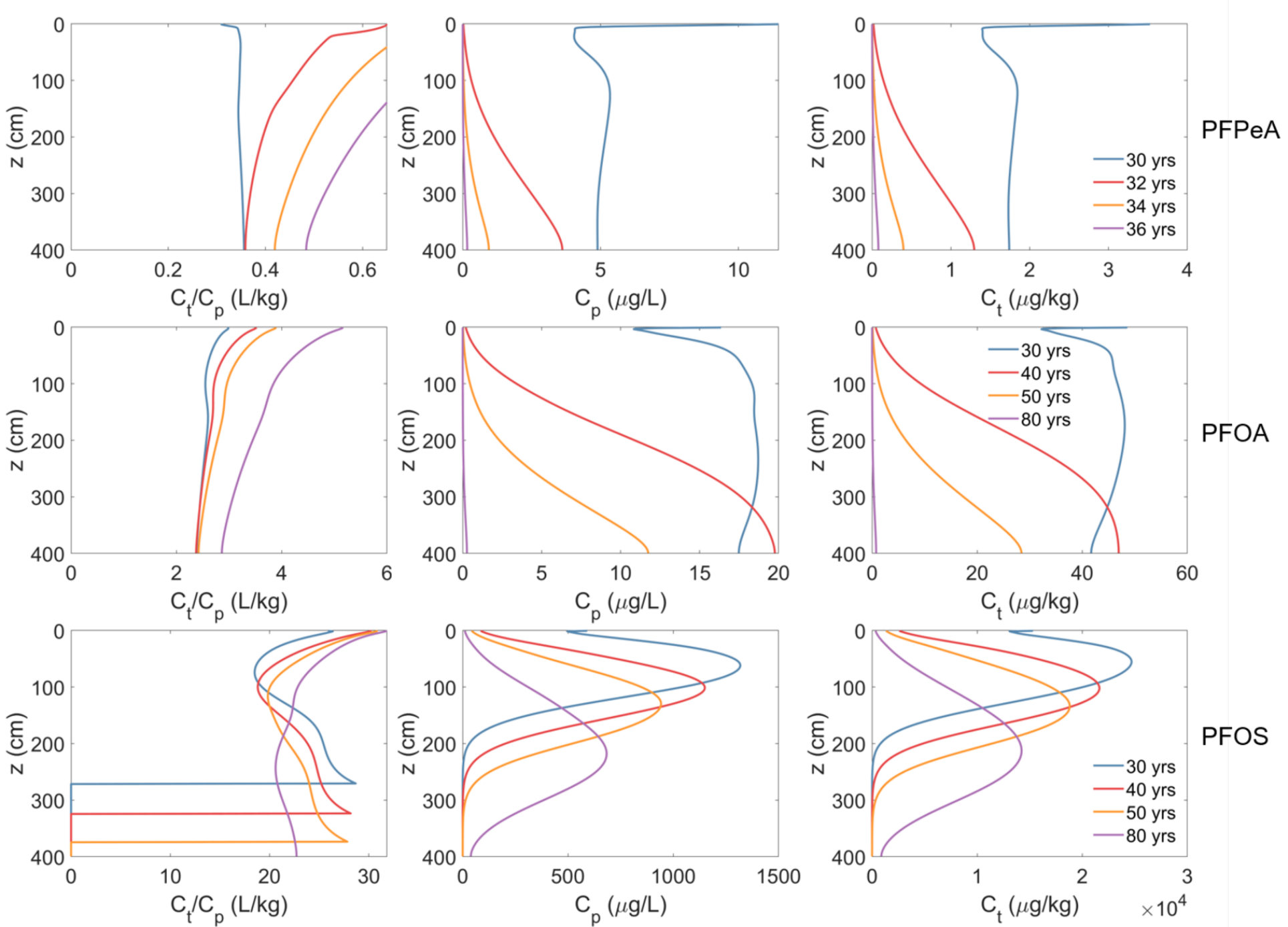
PFPeA
PFOA
PFOS
z (cm)
C_t/C_p (L/kg)
C_p (μg/L)
C_t (μg/kg)
30 yrs
32 yrs
34 yrs
36 yrs
40 yrs
50 yrs
80 yrs
$\times 10^4$

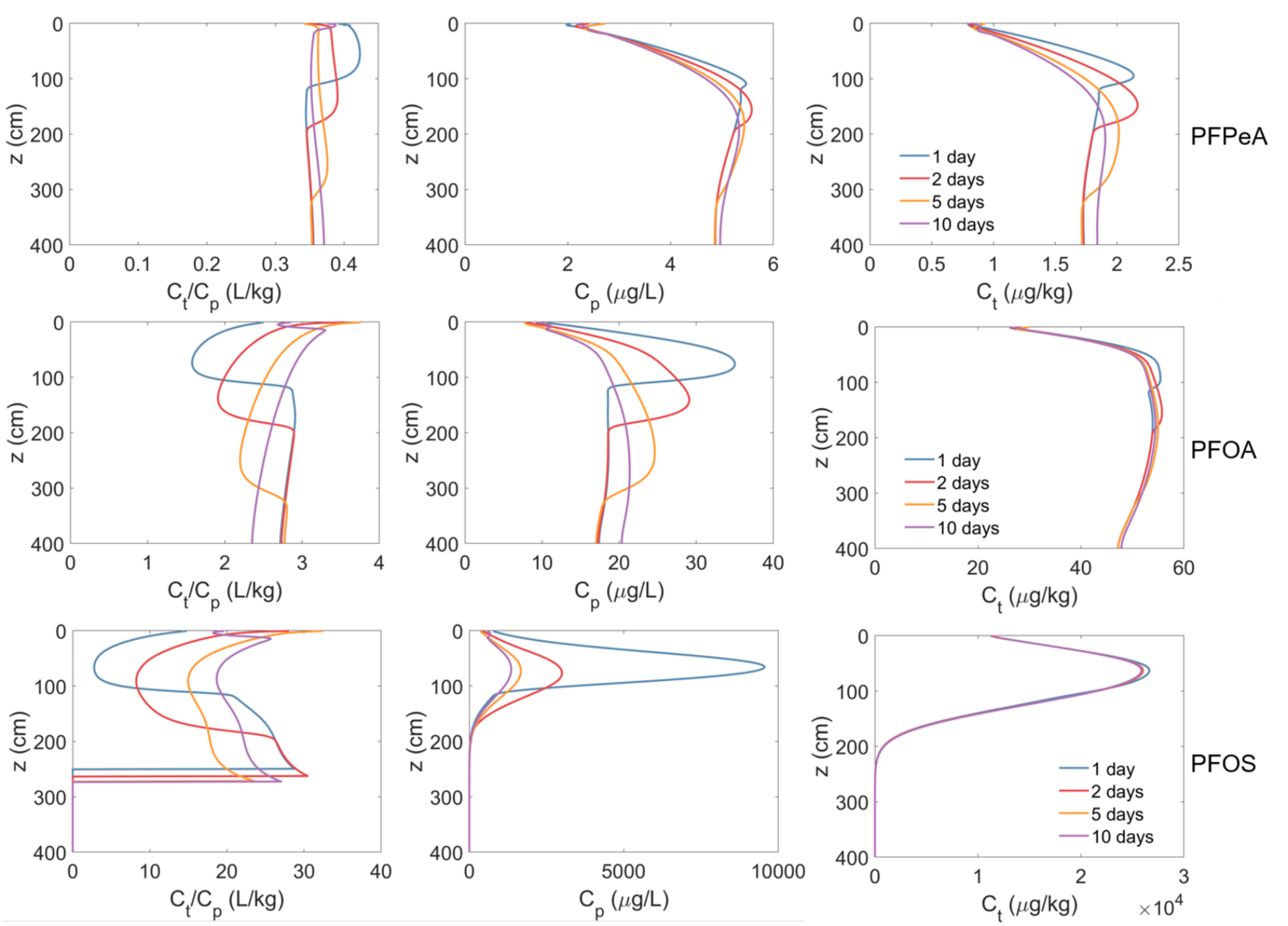
PFPeA
PFOA
PFOS
z (cm)
C_t/C_p (L/kg)
C_p (μg/L)
C_t (μg/kg)
1 day
2 days
5 days
10 days
$\times 10^4$

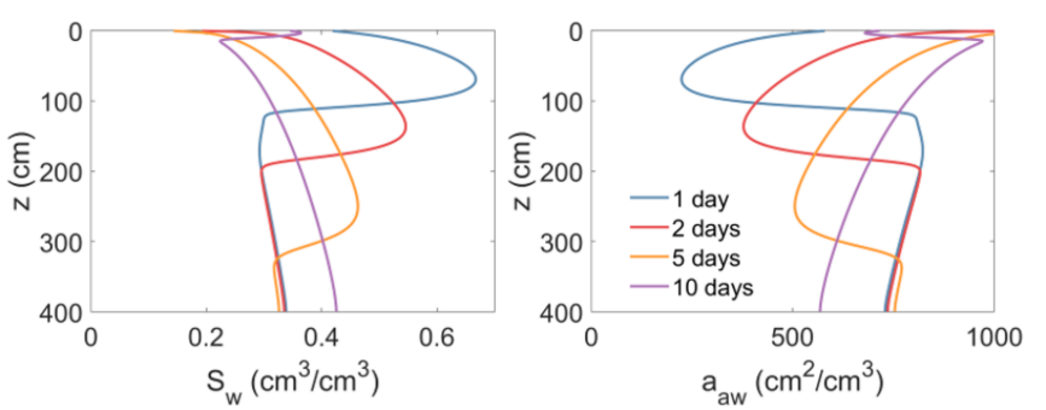
0
100
200
300
400
z (cm)
0
0.2
0.4
0.6
S_w (cm^3/cm^3)
0
500
1000
a_{aw} (cm^2/cm^3)
1 day
2 days
5 days
10 days

Porewater Concentration versus Total Soil Concentration

$$\frac{C_t}{C_p} = \frac{\theta_w}{\rho_b} R_d$$

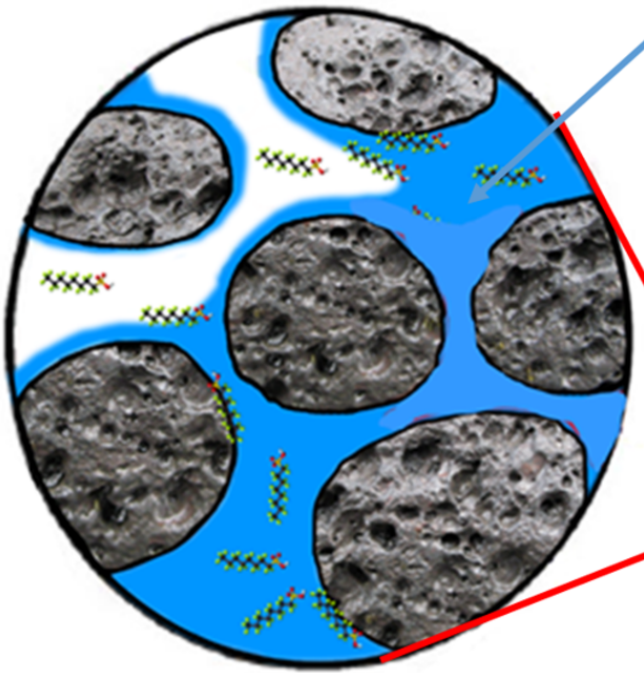

Porewater Concentration (C_p)

Solid

Water

Air

PFAS

*Not to scale

Total Soil Concentration (C_t)